Novel Multistage Three-Dimensional Medical Image Segmentation: Methodology and Validation

Lixu Gu, *Member, IEEE*, Jianfeng Xu, and Terence M. Peters, *Senior Member, IEEE*

***Abstract*—In this paper, we propose a novel multistage method for three-dimensional (3-D) segmentation of medical images and a new radial distance-based segmentation validation approach. For the 3-D segmentation method, we first employ a morphological recursive erosion operation to reduce the connectivity between the region of interest and its surrounding neighborhood; then we design a hybrid segmentation method to achieve an initial result. The hybrid approach integrates an improved fast marching method and a morphological reconstruction algorithm. Finally, a morphological recursive dilation is employed to recover any lost structure from the first stage of the multistage method. This approach is tested on 12 CT and 3 MRI images of the brain, heart, and kidney, to demonstrate the effectiveness and accuracy of this technique across a variety of imaging modalities and organ systems. In order to validate the multistage segmentation method, a novel radial distance-based validation method is proposed that uses a global accuracy (GA) measure. The GA is calculated based on local radial distance errors (LRDE), where LRDE are calculated on the radii emitted from points along the skeleton of the object rather than the centroid, in order to accommodate more complicated organ structures. The experimental results demonstrate that the proposed multistage segmentation method is fast and accurate, with comparable performance to existing segmentation methods, but with a significantly higher execution speed.**

***Index Terms*—Fast marching, local radial distance errors (LRDE), medical image, morphological reconstruction, radial distance-based validation (RDBV), segmentation.**

I. Introduction

ONE of the basic problems in medical imaging is to precisely segment structures of interest from a huge dataset, accurately represent them, efficiently visualize them, and perform measurements appropriate for diagnosis, surgery, and therapy guidance, or other applications [1], [2]. The most current segmentation algorithms applied to medical imaging problems only detect the rough boundaries of the structures in two dimensions (2-D), and so do not satisfy the requirements of many medical applications which require high accuracy. The continuing evolution of computer-aided diagnosis, image-guided and robotically assisted surgery, mandates the development of efficient, accurate three-dimensional (3-D) segmentation procedures.

Segmentation techniques can be divided into classes in many ways [3], [4], according to different classification schemes; however, model-based and region-based techniques represent the two main groups [5]. Model-based procedures include level set methods (as well as fast marching methods) proposed by Osher and Sethian [6] and the balloon method [7]. These techniques are based on deforming an initial contour or surface towards the boundary of the object to be detected. The deformation is obtained by minimizing a customized energy function such that its local minima are reached at the boundary of the desired structure. Some of these algorithms, such as the balloon method, are generally fast and efficient, but they sometimes fail to find the desired boundary for the following reasons.

- Since the stopping term of the deformation evolution depends on the image gradient flow being approximately zero, this often forces the contours to stop several voxels away from the desired boundary. Thus, the active contour sometimes does not match the boundary of the structure accurately, especially in regions with steep curvature and low gradient values.
- Since a surface tension component is incorporated into the energy function to smooth the contour, it also prevents the contour from fully propagating into corners or narrow regions. Increasing the number of sample nodes along the contour can improve the situation, but at a significant increase of computation time.
- The existence of multiple minima and the selection of the elasticity parameters can affect the accuracy of the results significantly.

Region-based algorithms include region growing [8], morphological reconstruction [9] and watershed [10]. Since these procedures are generally based on neighborhood operations, they examine each pixel during the evolution of the edge, so the results are usually very accurate. On the other hand, although region-based algorithms are several optimized algorithms in the literature [11], [12], they are generally computationally expensive.

In this paper, we propose a new 3-D multistage segmentation method based on an improved fast marching method and a morphological reconstruction, which performs the segmentation rapid and precise. A flow chart of our multistage method is shown in Fig. 1.

In the development of segmentation algorithms, good validation techniques are essential. Several validation methods have been proposed, for instance: similarity index (SI) [13], relative difference degree (RDD), relative overlap degree (ROD) [14],

Manuscript received July 4, 2005; revised December 18, 2005. This work was supported in part by the Chinese Natural Science Foundation under Grant 60571061, in part by the STCSM International Research Fund 045107045, and in part by the Ontario Research and Development Challenge Fund, Canada.

L. Gu and J. Xu are with the Image Guided Surgery and Therapy Laboratory, Department of Computer Science/School of Software, Shanghai Jiao Tong University, Shanghai 200030, China (e-mail: gu-lx@cs.sjtu.edu.cn; jxu9@uiuc.edu).

T. M. Peters is with the Imaging Research Laboratories, Robarts Research Institute, London, ON N6A 5K8, Canada and also with the University of Western Ontario, London, ON N6A 5B8, Canada (e-mail: tpeters@imaging.robarts.ca).

Digital Object Identifier 10.1109/TITB.2006.875665

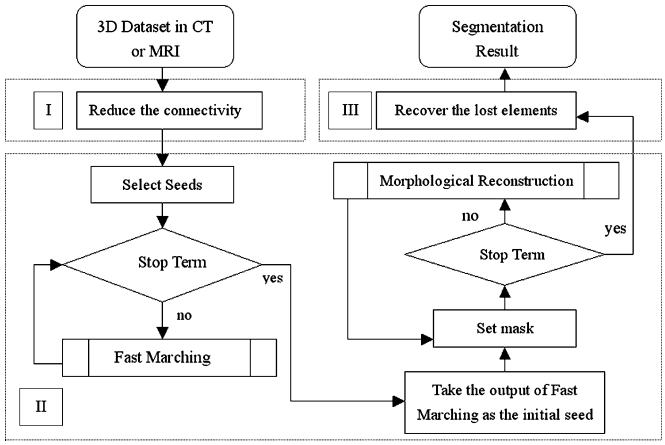

Fig. 1. Flowchart of the multistage method. Step I: Reduce the connectivity between the ROI and the neighboring tissues. Step II: Hybrid segmentation phase. After the improved fast marching method is employed to prepare a good initial seed, the morphological reconstruction is implemented. Step III: Recover the data elements of the ROI lost in stage I.

root-mean-squared error (RMSE) [15], and the method proposed by Chalana and Kim [16]. However, reliable validation of segmentation methods is still an open question. Besides the lack of acceptable gold standards, there are several challenges.

- Universality: A robust validation method should accommodate the variety of organ structures. Taking the RMSE method for instance, it always fails in the complex-shaped boundaries of the organ.
- Strictly monotony: The more accurate the segmentation is, the better results should be measured by the validation method. Some traditional validation methods, such as SI, RDD and ROD, could not meet the requirement. We will discuss this in Section IV-C.
  - *Synthesis:* A good validation method should both measure the local errors and the global error. Most existing methods only provide a partial measure.
  - *Applicability:* In addition to being theoretically effective, a good validation method should be easy to implement for practical applications.
  - *Quantitative:* The validation measure should produce a quantitative measure of whether the segmentation is acceptable or not, where the acceptable criteria should be based on different application purposes. The method proposed by Chalana and Kim [16] did not build quantitative measures for image quality.

In this paper, we present a novel radial distance-based validation (RDBV) method that can quantify both the local errors and the global accuracy between the segmented result and the gold standard. Our algorithm addresses all of the challenges described above.

The remainder of this paper is organized as follows: In Section II, we present a brief review of improved fast marching method and 3-D morphological reconstruction techniques, while in Section III, we describe the proposed multistage segmentation method. Then, we focus on the novel validation method RDBV in Section IV. Experimental results are given in Section V.

II. Fast Marching and 3-D Morphological Reconstruction

A. Level Set, Fast Marching

The level set method [17] is an interface propagation algorithm that represents a curve as the *zero level set* of a function one dimension (1-D) higher than original. Instead of tracing the interface itself, the level set method builds the original curves (so-called *front*) into a level set surface $\boldsymbol{\phi}$ (a hypersurface), where the front propagates with a speed $\boldsymbol{F}$ in its normal direction. To avoid complex contours, the current front $\boldsymbol{\phi}(x, y, t = i)$ is always set at zero height $\boldsymbol{\phi} = \mathbf{0}$. Hence, the level set evolution equation for the moving hypersurface can be presented as a Hamilton–Jacobi equation

$$\boldsymbol{\phi}_t + F|\nabla\phi| = 0. \tag{1}$$

The benefit of employing this "one-dimension-higher" concept is that even though the front (zero level set $\boldsymbol{\phi} = \mathbf{0}$) can become wildly contorted, the level set surface $\boldsymbol{\phi}$ will always be well behaved. All the complicated problems of contour breaking and merging are easier to handle in the higher dimension. A full discussion of these concepts is beyond the scope of this paper; instead the reader is referred to [17] or Sethian's web page.[1]

The level set method is designed for problems in which the speed function can be positive in some places and negative in others, so that the front can move both forwards and backwards.

The fast marching method [17] is a special case of the level set approach. Suppose we now restrict the front to propagate with a speed F, which is either always positive or always negative. This restriction allows us to simplify the level set formulation. If we assume $T(x, y)$ to be the time when the curve crosses the point (x, y), the surface $T(x, y)$ satisfies an Eikonal equation where the gradient of surface ∇T is inversely proportional to the speed of the front F

$$|\nabla T|F = 1. \tag{2}$$

The fast marching method is designed for problems in which the speed function never changes the sign, so that the front is always moving forward or backward and the front crosses each pixel or point only once. This restriction makes the fast marching approach much faster than the more general level set method.

However, sometimes the fast marching method results in an overflow, because of noise along the edge of ROI [18]. To prevent the front propagation from showing such behavior, we introduce global information [19] about the front into the speed function. Firstly, we define an average energy of the front $E_{\text{front}}(t)$ as

$$E_{\text{front}}(t) = \frac{1}{N_{\text{front}}} \sum_{(x,y,z)\in\Gamma(t)} E(x, y, z) \tag{3}$$

where $\Gamma(t)$ is the zero level set of the level set function, N presents the number of points along the contour and $E(x, y, z)$

[1] http://math.berkeley.edu/∼sethian/Explanations/level_set_explain.html

is the image energy at (x, y, z)). In the image $I(x, y, z)$), it is defined as

$$E(x, y, z) = -|\nabla G_\delta * I(x, y, z)| \tag{4}$$

where G_δ is a 3-D Gaussian function with a standard deviation δ. ∇ represents a gradient operation. And $E_{\text{front}}(t)$ is associated with the energy of all the points in the front. We introduce $E_{\text{front}}(t)$ into the speed function F and redefine it as

$$\begin{aligned} F(x, y, z, t) &= F(x, y, z) \cdot \exp(\beta E_{\text{front}}(t)) \\ &= F(x, y, z) \exp\left[-\beta \frac{1}{N_{\text{front}}} \right. \\ &\quad \left. \times \sum_{(x,y,z \in \Gamma(t))} |\nabla G_\delta * I(x, y, z)| \right], \quad \beta > 0. \end{aligned} \tag{5}$$

When most points along the front approach to the object edge, $E_{\text{front}}(t)$ becomes much smaller than 0, which results in $F(x, y, z, t)$ close to 0 to stop the front propagation. By changing the speed function from $F(x, y, z)$ to $F(x, y, z, t)$, the front can efficiently be prevented from overflowing.

In order to compute segmentation fast, we employ the improved fast marching method in our multistage method to perform the initial propagation of a contour from a user-defined seed to an approximate boundary.

B. 3-D Morphological Reconstruction

Mathematical morphology is a powerful methodology for the quantitative analysis of geometrical structures. We employ the standard technologies of recursive erosion, recursive dilation, and morphological grayscale reconstruction. More details can be found in [20] and [21].

We define a 3-D image f as a subset of the 3-D Euclidean space ($F \in \mathbf{R}^3$) and a 3-D structuring element $K \in \mathbf{R}^3$. The two basic operations can be defined as follows.

Dilation

$$\begin{aligned} D(m, n) &= F \oplus_g K \\ &= \max_{[a,b] \in K} \{F(m + a, n + b) + K(a, b)\}. \end{aligned} \tag{6}$$

Erosion

$$\begin{aligned} E(m, n) &= F \otimes_g K \\ &= \min_{[a,b] \in K} \{F(m - a, n - b) - K(a, b)\}. \end{aligned} \tag{7}$$

Recursive dilation, recursive erosion, and morphological reconstructions [9] as defined below are based on two basic operations

Recursive dilation

$$(F \oplus_g^i K) \begin{cases} F, & \text{if } i = 0 \\ (F \oplus_g^{i-1} K) \oplus_g K, & \text{if } i \geq 1. \end{cases} \tag{8}$$

Recursive erosion

$$(F \otimes_g^i K) \begin{cases} F, & \text{if } i = 0 \\ (F \otimes_g^{i-1} K) \otimes_g K, & \text{if } i \geq 1. \end{cases} \tag{9}$$

Morphological reconstruction

$$B_i = (B_{i-1} \oplus_g K) \cap |f|_G (B_i \in R^3, \quad i = 1, 2, \ldots). \tag{10}$$

In the equation above, i is a scale factor and K is the basic structuring element (e.g., 1 pixel radius disk). $\oplus_g$ denotes a dilation operation in grayscale, and $|f|_G$, represents the *mask* of the operation, resulting from a threshold operation using a gray level G by OTSU threshold which is a histogram analysis method. The iteration in (10) is repeated until the difference measured in pixels between B_{i-1} and B_i is falling below some small user-defined threshold value. In our experiment, the threshold value is between 50 and 300, depending on the size of the dataset. Since typical clinical 3-D data have millions of pixels, and the choice of the stop threshold only has hundreds pixels in difference, even a threshold of 300 has almost no effect on the accuracy of the result.

Morphological reconstruction is a very accurate method to recover an object on a pixel-by-pixel basis.

III. Multiage Segmentation Approach

Although the improved fast marching method is computational fast, it does not accurately cover the desired boundary, as described in Section II-A. Using the output of the improved fast marching method as the initial seed, the morphological reconstruction process is fast while maintaining its accuracy. Thus, our multistage method can make full use of the speed of the improved fast marching method, as well as the accuracy of the morphological reconstruction approach.

As shown in Fig. 1, the procedure includes three stages.

Stage 1. *Reduce the connectivity between ROI and the neighboring tissues*. Recursively erode the input 3-D image using a structuring element base (e.g., a sphere with 1 pixel radius) until the ROI is completely separated from the neighboring tissues, as determined by the operator. In most cases, connectivity between the ROI and the neighboring tissues may be heavily reduced by using recursive erosion. However, in the case that large areas between the ROI and the neighboring tissues are connected, recursive erosion is ineffective and the traditional fast marching method overflows. In order to make the multistage method robust, we had to improve the traditional the fast marching as described in Section II-A.

Stage 2. *Perform the hybrid segmentation*. Initially, the fast marching method is employed to quickly propagate the user-defined seed to a position close to the boundary. Then taking the output of the improved fast marching algorithm as the initial seed, morphological reconstruction is used to refine the initial seed as a "final check."

Stage 3. *Recover the lost data elements from stage 1*. During the recursive erosion in stage 1, parts of the object (usually around the edges) are often eliminated. To recover these lost components, the recursive dilation method is used. The reconstructed object surface is dilated recursively using the same

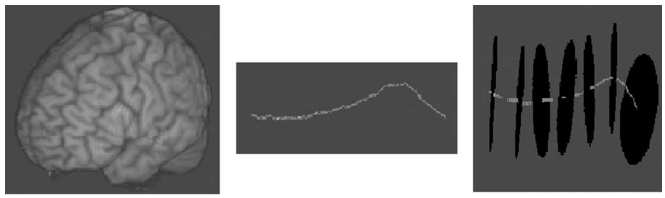

(a) (b) (c)

Fig. 2. Skeleton and radial construction. (a) Object (brain). (b) The curve denotes the skeleton computed by distance mapping method. (c) Radius construction. Black lines in (c) stand for the radials extended from a point along the skeleton.

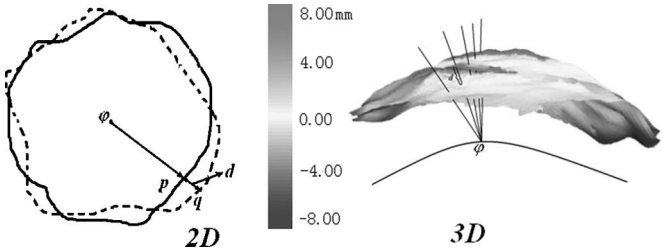

Fig. 3. LRDE. A particular radius φq intersects with S and G resulting in the intersection points q and p, respectively. d denotes the LRDE along the φq. The curve in the right figure stands for the skeleton of the object.

number of iterations as recorded in stage 1, which recovers the object surface to the "original" position. We note that the resulting image will in general not correspond exactly to the "original" image, but be smoothed, because the erosion, followed by dilation, corresponds to an "opening" operation. It nevertheless removes most of the noise surrounding the desired boundary. However, if we use a sphere with a 1-pixel radius as the structuring element, and use a small number of iterations to reduce the connectivity, the surfaces of smooth convex structures may be recovered accurately.

IV. Validation Method

A. Skeleton and Radial Construction

To compare the multistage method with the existing methods, a novel RDBV method is proposed, where the radii are emitted from the points along the skeleton of the object (Fig. 2).

We first calculate the skeleton of the object, using one of the many skeleton algorithms available from the literature, including manual extraction [22], topological thinning [23], distance mapping [24], etc. In our validation method, we use the distance mapping method to extract the skeleton, and then construct the radii that extend from the points along the skeleton of the object.

As shown in Fig. 3, φ is a point along the skeleton. From this point, we construct sufficient equispaced radii planes perpendicular to the skeleton line. Each radial line intersects the surfaces of segmented region S, the corresponding ground truth image G, with the intersection points q and p, respectively. As shown in Fig. 3, we define $d = \varphi q - \varphi p$ as the local radial distance error (LRDE). If we apply the radial construction method to every point along the skeleton, we could obtain LRDE over the entire surface region.

B. Framework of RDBV

Points along the skeleton are numbered in order as $\phi_0, \phi_1, \phi_2, \ldots, \phi_{N-1}$, where N represents the number of points along the skeleton. Furthermore, radial lines emitted from the point ϕ_i are denoted as $\mathbf{R}_{i0}, \mathbf{R}_{i1}, \mathbf{R}_{i2}, \ldots, \mathbf{R}_{iM-1}$, where M is the number of radii emitted from ϕ_i, and the intersection points on the surfaces S and G are presented as $q_{i0}, q_{i1}, q_{i2}, \ldots, q_{iM-1}$ and $p_{i0}, p_{i1}, p_{i2}, \ldots, p_{iM-1}$, respectively. The choices of M and N depend on the resolution of the origin 3-D data. Assume the extent and the spacing of the data are (E_x, E_y, E_z) and (S_x, S_y, S_z), respectively. l denotes the length of the skeleton. In our experiment, we define M and N as

$$N = l/\min\{S_x, S_y, S_z\} \tag{11}$$

$$M = t \times \max\{E_x, E_y, E_z\} \tag{12}$$

where $t = 4$, as at most four faces of the origin data solid could intersect with the radii emitted from certain point.

Thus, the LRDE can be defined as

$$d_{ij} = \phi_i q_{ij} - \phi_i p_{ij}, \qquad 0 \le i \le N-1; \quad 0 \le j \le M-1. \tag{13}$$

We can define c_{ij}, which reflects the degree of under-segmentation or over-segmentation along the direction of R_{ij}

$$c_{ij} = \left| \frac{d_{ij}}{\phi_i p_{ij}} \right|, \qquad 0 \le i \le N-1; \quad 0 \le j \le M-1. \tag{14}$$

Then, we place c_{ij} into one of following three categories:

- $0 < c_{ij} \le \frac{1}{k}$ (local segmentation is considered accurate);
- $\frac{1}{k} \le c_{ij} < \frac{2}{k}$ (local segmentation is not accurate);
- $c_{ij} \ge \frac{2}{k}$ (local segmentation is unacceptable);

where k is a constant integer. After consultation with radiologists, it was concluded that $c_{ij} \le 0.05$ could be recommended as an acceptable accurate local segmentation result, and thus k may be set to a value of 20. We introduce the concept of global accuracy (GA) that reflects the accuracy of global segmentation and define it as

$$\mathrm{GA} = NM \left[\sum_{i,j=0}^{N-1,M-1} L_{i,j} \right]^{-1} \qquad (0 \le i \le N-1, 0 \le j \le M-1) \tag{15}$$

where the target function L_{ij} (see Section IV-C) is defined as

$$L_{ij} = \lambda^{c_{ij}\,k}, \qquad 0 \le i \le N-1; \quad 0 \le j \le M-1. \tag{16}$$

According to the definition of GA, we conclude that the higher the value of GA is, the more accurate the segmentation. Since $L_{ij} \le 1/k (0 \le i < N, 0 \le j < M)$ is considered as an accurate segmentation, we can define GA_t, the threshold value of GA, as

$$GA_t = NM \left[\sum_{i,j=0}^{N-1,M-1} \lambda^{k \times \frac{1}{k}} \right]^{-1} = 0.65, \qquad 0 \le i \le N-1; \quad 0 \le j \le M-1. \tag{17}$$

Thus, segmentations for which $GA \ge GA_t = 0.65$ may be considered as an acceptable segmentation in RDBV.

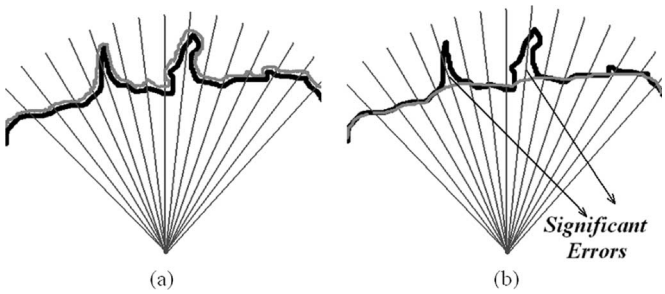

Fig. 4. Evaluation of two typical segmentation results [(a) acceptable and (b) unacceptable] based on the LRDE that is the distance between the gray and black curves. In (a) and (b), the black curves stand for the contours of the "gold standard," while the gray curves denote the contours of the segmented results. However, the simple total errors that may result are equal for both cases.

C. Advantage of Target Function L_{ij} and its Coefficient λ

In the Section I, "strictly monotony" is mentioned as a challenge for a validation method and most of the existing validation methods can hardly meet the criteria. That is to say, high local error may result in a low global error in some special cases, such as the next example.

As shown in Fig. 4, two different segmentation results are depicted. Fig. 4(a) shows a result that is clearly superior to that in 4(b), since the latter one has significant local errors, which always means some parts of the object boundary are lost. In this case, because the simple total errors may be equal, it is possible for traditional validation methods, such as SI, to return an acceptable result, even if the segmentation is clearly in error. The RDBV, on the other hand, can distinguish these cases by introducing the target function L_{ij} and its coefficient λ.

In GA, we design a target function $L_{ij} = \lambda^{c_{ij}k}$ to penalize (enlarge) local significant inaccuracy. Meanwhile, the target function should satisfy the following conditions:

$$\begin{cases} \dfrac{dL_{ij}}{d(c_{ij}k)} < 1, & 0 \le c_{ij} < \frac{2}{k} \\ \dfrac{dL_{ij}}{d(c_{ij}k)} = 1, & c_{ij} = \frac{2}{k}, \quad 0 \le i \le N-1; \quad 0 \le j \le M-1 \\ \dfrac{dL_{ij}}{d(c_{ij}k)} > 1, & 0.2 > c_{ij} > \frac{2}{k}. \end{cases} \tag{18}$$

From $dL_{ij}/d(c_{ij}k) = 1, \quad c_{ij} = 2/k$, we get an equation in λ

$$\ln \lambda \times \lambda^2 = 1. \tag{19}$$

From which we conclude $\lambda = 1.54$.

The advantages of the target function are described as follows.

- $0 \le c_{ij} \le \frac{2}{k}$: Local segmentation is regarded as accurate or acceptable. (As shown as dotted curve in Fig. 5, the curve of the target function L_{ij} is nearly flat). This will gradually increase the weight factor to the GA.
- $\frac{2}{k} < c_{ij}$: Target function changes quickly with the increasing of the combined variable $c_{ij}k$ (shown as a solid curve in Fig. 5). By strongly increasing the weight factor, this can penalize the inaccuracy to an unacceptable extent.

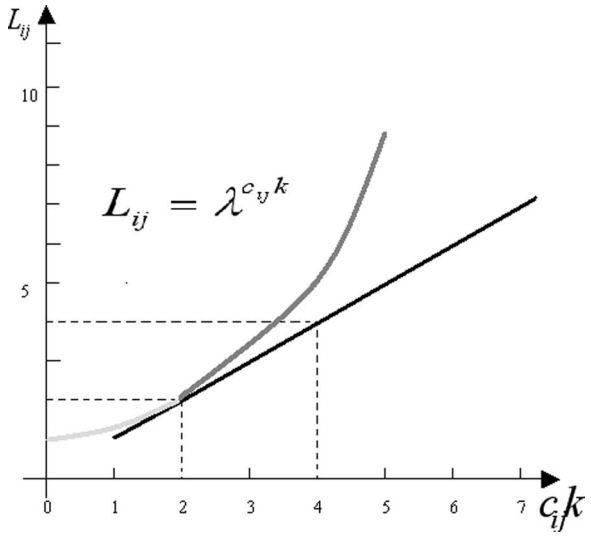

Fig. 5. Target function $L_{ij}(k = 20)$ is designed to penalize the significant inaccuracy in RDBV.

Based on this penalized-inaccuracy target function, the proposed RDBV can distinguish the segmentation results presented in Fig. 4.

V. Experimental Results

A. Software and Source Data

Our segmentation environment, "TkSegmentation," was written in Python, and extensive uses the visualization toolkit (VTK)[2] and insight toolkit (ITK)[3] classes, which provided the implementations for the algorithms of fast marching, morphological reconstruction, watershed and the our multistage method. In our experiment, the watershed is interactive with a top-down gradient descent strategy [25].

In order to test the robustness and universality of our multistage method, our source data cover different modalities and different typical organs in the human body including the brain, heart and kidney.

In our experiments, we used three different MRI scans of the brain. One of the three brain MRI datasets is the standard CJH27 $181 \times 217 \times 181$ voxel image volume derived from an average of 27 T1 weighted images of a normal brain [26] and its gold standard is available.[4] This gold standard could be used directly in the validation. To cover different modality, the other two T2 weighted neurological MRI datasets are $256 \times 256 \times 124$ volumes. Cardiac segmentation is very difficult because of its complex structure. Our source data includes one group of canine CT datasets. The data contain a dynamic volume, acquired with a gated acquisition technique on an 8-slice GE helical CT scanner, consisting of 86 slices at each of ten equally spaced snapshots during the cardiac cycle. The images were each 512×512 pixels (0.35 mm $\times$ 0.35 mm), with an axial spacing of 1.25 mm. Two CT datasets were used in the kidney example and they are both

[2]www.vtk.org
[3]www.itk.org
[4]http://www.bic.mni.mcgill.ca/brainweb/

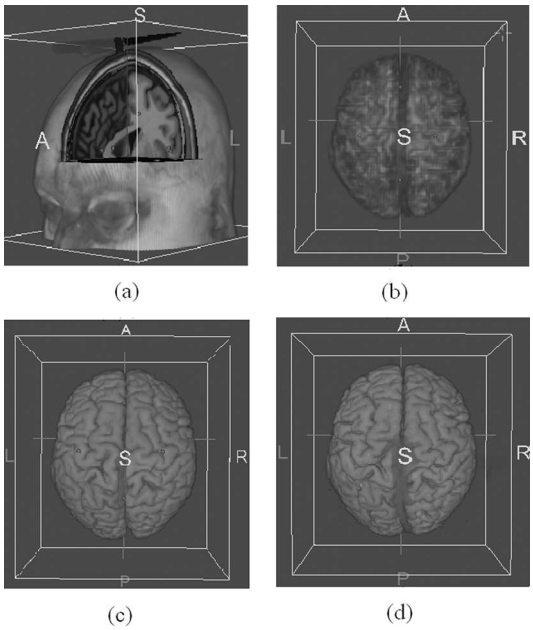

Fig. 6. Examples of segmented brains. (a) Source Data (CJH27). (b)–(d) The segmentation results of fast marching, the multistage method, and the watershed, respectively.

comprised of 417×175 (0.35 mm) ^{2} pixels per slice, and 101 slices equispaced with 1.25 mm.

We applied our multistage segmentation method to all of the 15 volume datasets. A 2-GHz Pentium-4 PC, 512-MB memory desktop computer running Windows-XP was employed to run the segmentation. All the brain images, three of the heart datasets, and both the kidney volumes were employed in the validation. The results of these experiments are described below.

B. Case Study

1) Brain Images: We applied our algorithm to one T1 and two T2 weighted MRI head scans, comparing with the fast marching method, morphological reconstruction, and watershed. In general, watershed and our multistage method, as well as morphological reconstruction, can segment the ruga of the cortex well [Fig. 6(c) and (d)], while fast marching could not deal with this kind of data accurately [Fig. 6(b)].

Tables I and II show the quantitative accuracy employing RDBV and the computing cost of the segmentation result, respectively. The multistage method requires 20 s more than the fast marching method, but it achieved a better GA measure of 0.830 averagely; it is also approximately three or four times faster than the morphological reconstruction with similar accuracy. Among all these methods, watershed is regarded as the most accurate with a GA of 0.883 in average. However, its computation time is about four to six times more than our multistage method (Table II). Moreover, the high accuracy of watershed depends on more human interactions and experience on anatomical structures in the final merging stage.

2) Heart Images: One dynamic CT scan of a beating heart, containing ten individual volumes throughout the cardiac cycle, was used in this study. These images were segmented individually. The segmentation of a beating heart is more difficult than a brain due to the more complex anatomy, as well as the presence of the artifacts and nonisotropic image resolution, but our multistage method handled the data in a robust manner, in spite of such potential problems. Besides, there are always some connections between heart and some other tissues, which lead to oversegmentation. The first stage of our algorithm is designed to solve this problem and it actually worked out as expected on the heart (Fig. 7).

The average segmentation time for the ten volumes is 131.1 s (Table II), which is longer than for the brain, due to the additional time required to segment the blood vessels. However, if the blood vessels are removed early in preprocessing, computation time is reduced considerably. Fast marching could not handle the connections and blood vessels very well, while watershed is adept on them [Fig. 8(II)], but more interactions are involved. The multistage method, as well as the morphological reconstruction, can avoid large areas with significant local error [Fig. 8(II)]. According to the metric of GA (Table I), we achieved similar trends as we had in the brain study.

TABLE I
GA MEASURE OF THE FAST MARCHING, MORPHOLOGICAL RECONSTRUCTION, PROPOSED MULTISTAGE METHOD, AND WATERSHED ON TESTING DATA SETS

Datasets	Fast Marching	Morphological Reconstruction	Proposed Multistage Method	Watershed
CJH27	0.695	0.822	0.823	0.882
Brain 1	0.676	0.829	0.828	0.878
Brain 2	0.712	0.835	0.838	0.889
average	0.694	0.829	0.830	0.883
Heart 1	0.661	0.775	0.775	0.918
Heart 2	0.694	0.788	0.786	0.968
Heart 3	0.674	0.781	0.787	0.942
Heart4	0.678	0.780	0.780	0.915
Heart5	0.649	0.791	0.789	0.937
Heart6	0.663	0.795	0.798	0.915
Heart7	0.667	0.794	0.795	0.912
Heart8	0.675	0.784	0.785	0.927
Heart9	0.687	0.789	0.794	0.912
Heart10	0.648	0.782	0.795	0.908
average	0.670	0.786	0.788	0.925
Kidney 1	0.767	0.912	0.920	0.985
Kidney 2	0.785	0.913	0.918	0.975
average	0.776	0.913	0.919	0.980

TABLE II
COMPUTING COST IN SECONDS OF THE FAST MARCHING, MORPHOLOGICAL RECONSTRUCTION, PROPOSED MULTISTAGE METHOD, AND WATERSHED ON TESTING DATA SETS

Datasets	Fast Marching	Morphological Reconstruction	Proposed Multistage Method	Watershed*
CJH27	16.3'	188.2'	45.8'	242.5'
Brain 1	16.1'	80.6'	34.5'	131.6'
Brain 2	16.4'	78.7'	31.8'	125.2'
average	16.3'	115.8'	37.4'	166.4'
Heart 1	66.9'	442.1'	120.8'	562.6'
Heart 2	68.7'	450.6'	116.6'	549.3'
Heart 3	67.4'	466.2'	137.0'	558.7'
Heart4	65.3'	422.6'	132.4'	533.6'
Heart5	65.0'	437.4'	122.0'	548.7'
Heart6	65.9'	411.0'	128.3'	557.8'
Heart7	66.4'	426.0'	135.6'	568.4'
Heart8	66.6'	436.5'	127.8'	560.5'
Heart9	67.6'	370.7'	133.4'	568.3'
Heart10	67.0'	409.3'	123.3'	561.5'
average	66.7'	427.2'	131.1'	556.9'
Kidney 1	8.26'	29.2'	19.6'	92.8'
Kidney 2	8.40'	32.4'	23'1'	97.7'
average	8.33'	30.8'	21.4'	95.3'

* In the experiment of watershed segmentation, the datasets of brain, heart and kidney are resampled with the magnification factor 1, 0.5 and 0.8 respectively.

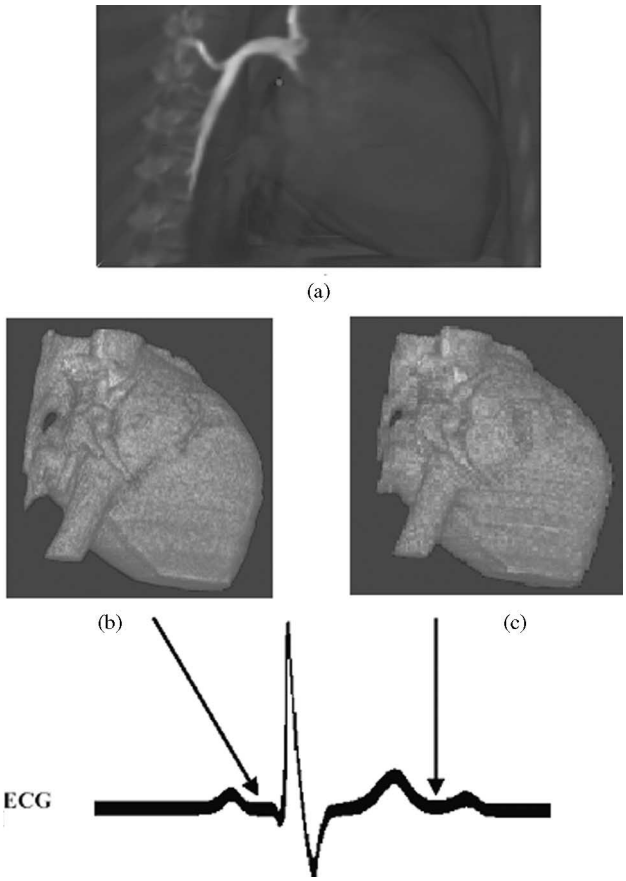

Fig. 7. Examples of two of the ten segmented heart volumes in a cardiac cycle. (a) Original dataset shown as a volume rendering. (b) Diastolic phase. (c) Systolic phase.

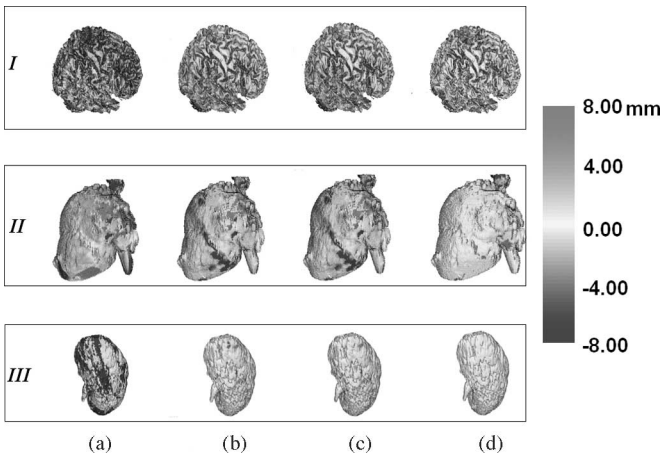

Fig. 8. LRDE distribution in segmentation results of the (a) fast marching, where color scale stands for LRDE, (b) morphological reconstruction, (c) multistage method, and (d) watershed on brains (I), hearts (II), and kidney (III).

3) Kidney Images: For the kidney example, we employed two CT datasets to test our approach. At the second stage (hybrid segmentation as illustrated in Fig. 1), we initiated the procedure using three seeds in each kidney to accelerate the processing. After the process was initiated, the resulting fronts in both kidney regions propagated independently and concurrently. As kidney's structure is simpler, the advantage of the multistage method over watershed is more obvious. The average GA values of our multistage method and watershed are 0.919 and 0.980, respectively, which reflects that our method is only slightly inferior to the watershed in accuracy, while our multistage method is five times faster than the watershed (Tables I and II). Moreover, the multistage method can easily segment the two kidneys simultaneously from the 3-D image (Fig. 9), where the traditional morphological reconstruction method is struggling.

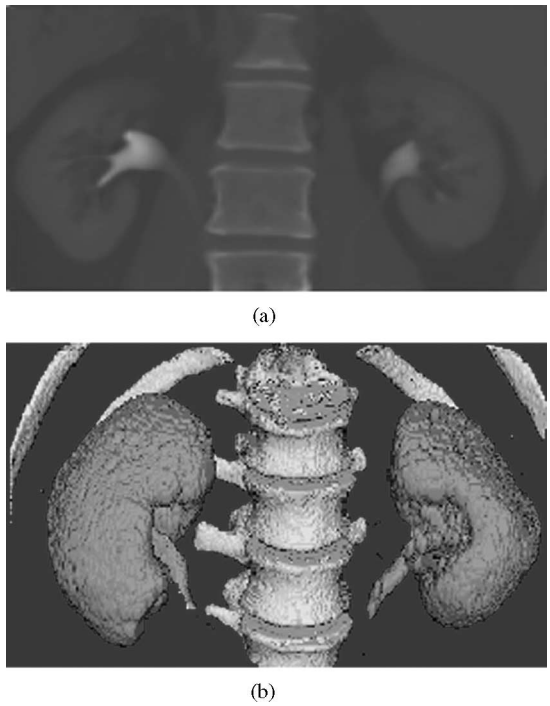

Fig. 9. Examples of the segmented kidney. (a) Source image. (b) A pair of kidneys segmented by the multistage method.

In conclusion, our multistage method improves the fast marching significantly in accuracy when keeps a high performance. Meanwhile, it is more repeatable and significantly reduces computing cost (around five times) with minor loss in accuracy compared to watershed. Moreover, its advantage over morphological reconstruction is also the much faster speed and simultaneity in segmenting different human parts, such as the left and right kidneys.

VI. Conclusion

We have presented a new, fully 3-D, reliable segmentation approach for visualization using a fast multistage method. Although it is slower than the fast marching method, it offers significantly improved accuracy. Compared to the morphological reconstruction and watershed it is superior in means of computing cost while maintaining a high accuracy. The approach takes advantage of the speed and accuracy of both model-based and region-based segmentation methods. It was tested on fifteen 3-D image volumes in a variety of application studies and image modalities. Meanwhile, a novel validation method (RDBV) was proposed to improve measurement of segmentation results

using both local and global information. Quantitative validation demonstrated an average value of GA over different kinds of organs (as measured by RDBV). As the future work, we plan to get more segmentation results performed manually by multiple experts, as the gold standard is still manual segmentation by an expert. A histogram of LRDE could help to understand our validation method better.

ACKNOWLEDGMENT

The authors would like to thank S. Peng and G. Jiang for their great help in the watershed segmentation and distance mapping skeleton algorithm. They are also grateful to P. Bertram for proofreading the paper carefully and to Dr. S. Chang, Director of the Radiology Department of Shanghai Oriental Hospital, for his help in providing testing data and clinical advice. In addition, the authors wish to thank the editors and several anonymous reviewers of the IEEE TITB for their helpful comments.

REFERENCES

[1] Q. Zou, K. C. Keong, N. W. Sing, and Y. Chen, "MRI head segmentation for object based volume visualization," in *Proc. 7th Australia and New Zealand Intell. Inf. Syst. Conf.*, Perth, Australia, 2001, pp. 361–366.

[2] A. F. Frangi, W. J. Niessen, and M. A. Viergever, "Three-dimensional modeling for functional analysis of cardiac images: A review," *IEEE Trans. Med. Imag.*, vol. 20, no. 1, pp. 2–5, Jan. 2001.

[3] S. Lakare and A. Kaufman, "3D segmentation techniques for medical volumes," Research Proficiency Exam, Center Visual Comput., Dept. Comput. Sci., State Univ., Stony Brook, NY, Dec. 2000.

[4] J. C. Rajapakse, J. N. Giedd, and J. L. Rapopart, "Statistical approach to segmentation of single-channel cerebral MR Images," *IEEE Trans. Med. Imag.*, vol. 16, no. 2, pp. 176–186, Apr. 1997.

[5] J. S. Suri, "Computer vision, pattern recognition, and image processing in left ventricle segmentation: Last 50 years," *J. Pattern Anal. Appl.*, vol. 3, no. 3, pp. 209–242, 2000.

[6] S. Osher and J. A. Sethian, "Fronts propagating with curvature dependent speed: Algorithms based on Hamilton–Jacobi formulation," *J. Comput. Phys.*, vol. 79, pp. 12–49, 1988.

[7] C. Chen *et al.*, "Segmentation of arterial geometry from ultrasound images using balloon models," in *Proc. IEEE Int. Symp. Biomed. Imaging: Macro to Nano*, 2004, vol. 2, pp. 1319–1322.

[8] S. Wan and W. E. Higgins, "Symmetric region growing," *IEEE Trans. Image Process.*, vol. 12, no. 9, pp. 1007–1015, Sep. 2003.

[9] H. Fujimoto, L. Gu, and T. Kaneko, "Recognition of abdominal organs using 3D mathematical morphology," *Syst. Comput. Jpn.,* vol. 33, no. 8. pp. 843–850, 2002.

[10] A. Bieniek and A. Morga, "An efficient watershed algorithm based on connected components," *Pattern Recognit.*, vol. 33, pp. 907–916, 2000.

[11] F. Cheng and A. N. Venetsanopoulos, "Adaptive morphological operators fast algorithms and their applications," *Pattern Recog.*, vol. 33, pp. 917–933, 2000.

[12] V. Grau, A. U. J. Mewes, M. Alcaniz, R. Kikinis, and S. K. Warfield, "Improved watershed transform for medical image segmentation using prior information," *IEEE Trans. Med. Imag.*, vol. 23, no. 4, pp. 447–458, Apr. 2004.

[13] A. P. Zijdenbos, B. M. Dawant, R. A. Margolin, and A. C. Palmer, "Morphometric analysis of white matter lesions in MR images: Method and validation," *IEEE Trans. Med. Imag.*, vol. 13, no. 4, pp. 716–724, Dec. 1994.

[14] D. L. Collins, A. C. Evans, and C. Holms, "Automatic 3D segmentation of neuro-anatomical structures from MRI," in *Proc. Inf. Process. Med. Imag.*, De Berder, France, 1995, pp. 139–152.

[15] R. Pichumani, "Construction of a three-dimensional geometric model for segmentation and visualization of cervical spine images" Ph.D. dissertation, Stanford Univ., Stanford, CA, 1997.

[16] V. Chalana and Y. Kim, "A method for evaluation of boundary detection algorithm on medical images," *IEEE Trans. Med. Imag.*, vol. 16, no. 5, pp. 642–652, Oct. 1997.

[17] J. A. Sethian, *Level Set Methods and Fast Marching Methods*. Cambridge, U.K.: Cambridge Univ. Press, 1999.

[18] J. Xu and L. Gu, "Evaluation of morphological reconstruction, fast marching and a novel hybrid segmentation method," in *Proc. 1st Int. Symp. CIS 2004*, J. Zhang, J.- H. He, and Y. Fu, Eds. Shanghai, China, pp. 678–684.

[19] J. Yan and T. Zhuang, "Applying improved fast marching method to endocardial boundary detection in echocardiographic images," *Pattern Recognit. Lett.*, vol. 24, pp. 2777–2784, 2003.

[20] P. Dokladal, R. Urtasun, I. Bloch, and L. Garnero, "Segmentation of 3D heart MR images using morphological reconstruction under constraints and automatic selection of markers," in *Proc. Int. Conf. Image Process.*, 2001, vol. 3, pp. 1075–1078.

[21] L. Gu and T. Kaneko, "Extraction of organs using three-dimensional mathematical morphology," *Syst. Comput. Jpn.*, vol. 31, no. 7, pp. 29–37, 2000.

[22] Y. Ge, D. Stelts, and D. Vining, "3-D skeleton for virtual colonoscopy," in *Proc. 4th Int. Conf. Visualization in Biomedical Computing,* 1996, vol. 1131, pp. 449–454.

[23] F. Chang, Y. Lu, and T. Pavlidis, "Feature analysis using line sweep thinning algorithm," *IEEE Trans. Pattern Anal. Mach. Intell.*, vol. 21, no. 2, pp. 145–158, Feb. 1999.

[24] J. Jang and K. Hong, "A pseudo-distance map for the segmentation-free skeletonization of gray-scale images," in *Proc. Int. Conf. Computer Vision*, 2001, vol. 2, pp. 18–23.

[25] S. Peng and L. Gu, "A novel watershed method using second order gradient image," in *Proc. 19th Int. Congr. Exhibit. CARS2005*, Berlin, Germany, p. 1277.

[26] R. K. S. Kwan, A. C. Evans, and G. B. Pike, "MRI simulation-based evaluation of image processing and classification methods," *IEEE Trans. Med. Imag.*, vol. 18, no. 11, pp. 1085–1097, Nov. 1999.

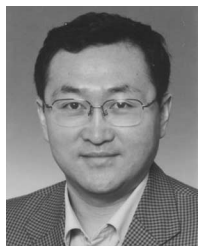

Lixu Gu (M'04) received the Ph.D. degree in computer science from the Toyohashi University of Technology, Toyohashi, Japan, in 1999.

After completing the Ph.D., he was with Robarts Research Institute, London, ON, Canada, for three years, working on image-guided surgery and therapy and was responsible for research and software development of medical image analysis. In 2003, he joined the research group in the Department of Computer Science, Shanghai Jiao Tong University, Shanghai, China, where he set up the Laboratory of Image Guided Surgery and Therapy and is currently the Director. He is also a Professor in the School of Software Engineering, Shanghai Jiao Tong University. He is the author of over 40 papers in related research areas. His research interests include pattern recognition, computer vision, medical image processing, computer graphics, and image-guided surgery and therapy.

Dr. Gu is a Social Chair and PC Member of the 27th IEEE EMBS Conference, Shanghai. He was awarded the Best Poster Award at the 17th Congress of Computer Assisted Radiology and Surgery (CARS), London, U.K., in 2003, and serves as a Program Committee Member of the CARS.

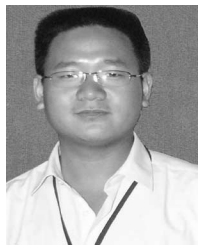

Jianfeng Xu received the B.Sc. degree in computer science from Xidian University, Xi'an, China, in 2003. He is currently working toward the M.Sc. degree in computer science at Shanghai Jiao Tong University, Shanghai, China.

His research interests include medical image segmentation and validation and soft tissue modeling.

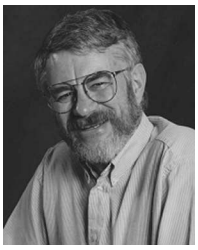

Terence M. Peters (M'64–SM'97) received the Ph.D. degree in electrical engineering from the University of Canterbury, Christchurch, New Zealand, in 1974.

He is currently a Scientist at the Imaging Research Laboratories, Robarts Research Institute (RRI), London, ON, Canada, and a Professor in the Departments of Radiology and Nuclear Medicine, and Medical Biophysics, University of Western Ontario, London, ON. At RRI, he established an image-guided surgery and therapy group. He has authored over 150 peer-reviewed papers and book chapters and has delivered over 130 invited presentations. For the past 20 years, his research has focused on the application of computational hardware and software to medical imaging modalities in surgery and therapy.

Dr. Peters is a Fellow of the Canadian College of Physicists in Medicine, Edmonton, AB, Canada. He serves as an Associate Editor of the IEEE TRANSACTIONS ON MEDICAL IMAGING. He is also a Member of the Editorial Boards of *Magnetic Resonance Imaging; Computer Methods in Biomechanics and Biomedical Engineering; Australasian Physical and Engineering Sciences in Medicine*; *Medical Image Analysis*; and *Current Medical Imaging Reviews*. He is an Executive Member of the Board as well as the Treasurer of the MICCAI society.